

Article

Simulation of Pan Evaporation and Application to Estimate the Evaporation of Juyan Lake, Northwest China under a Hyper-Arid Climate

Teng-Fei Yu ^{1,2,3} , Jian-Hua Si ^{1,2,3}, Qi Feng ^{1,2,3,*} , Hai-Yang Xi ^{1,2,3}, Yong-Wei Chu ⁴ and Kai Li ⁴

¹ Alxa Desert Eco-hydrology Experimental Research Station, Northwest Institute of Eco-Environment and Resources, Chinese Academy of Sciences, Lanzhou 730000, China; yutf@lzb.ac.cn (T.-F.Y.); jianhuas@lzb.ac.cn (J.-H.S.); xihy@lzb.ac.cn (H.-Y.X.)

² Key Laboratory of Eco-hydrology of Inland River Basin, Chinese Academy of Sciences, Lanzhou 730000, China

³ Gansu Hydrology and Water Resources Engineering Research Center, Lanzhou 730000, China

⁴ Heihe Water Resources and Ecological Protection Research Center, Lanzhou 730000, China; yutf08@lzb.ac.cn (Y.-W.C.); 18054186769@189.cn (K.L.)

* Correspondence: qifeng@lzb.ac.cn; Tel.: +86-931-496-7089

Received: 30 October 2017; Accepted: 5 December 2017; Published: 7 December 2017

Abstract: Because of its nature, lake evaporation (E_L) is rarely measured directly. The most common method used is to apply a pan coefficient (K_p) to the measured pan evaporation (E_p). To reconstruct the long sequence dataset of E_p , this study firstly determined the conversion coefficients of E_p of two pans ($\phi 20$ and E601, each applied to a different range of years) measured synchronously at the nearest meteorological station during the unfrozen period through 1986 to 2001, and then E_p was estimated by the PenPan model that developed to the Class A pan and applied to quantify the E_L of the Juyan Lake, located in the hyper-arid area of northwest China. There was a significantly linear relationship between the E601 and $\phi 20$ with the conversion coefficients of 0.60 and 0.61 at daily and monthly time scales, respectively. The annual E_p based on monthly conversion coefficients was estimated at 2240.5 mm and decreased by 6.5 mm per year, which was consistent with the declining wind speed (U) during the 60 years from 1957 to 2016. The E_p simulated by the PenPan model with the modified net radiation (R_n) had better performance (compared to E_p measured by E601) than the original PenPan model, which may be attributed to the overestimated R_n under the surface of E601 that was embedded in the soil rather than above the ground similar to the Class A and $\phi 20$. The measured monthly E_L and E_p has a significantly linear relationship during the unfrozen period in 2014 and 2015, but the ratio of E_p to E_L , i.e., K_p varied within the year, with an average of 0.79, and was logarithmically associated with U . The yearly mean E_L with full lake area from 2005 to 2015 was 1638.5 mm and 1385.6 mm, calculated by the water budget and the PenPan model with the modified R_n , respectively; the latter was comparable to the surface runoff with an average of 1462.9 mm. In conclusion, the PenPan model with the modified R_n has good performance in simulating E_p of the E601, and by applying varied K_p to the model we can improve the estimates of lake evaporation.

Keywords: pan evaporation; pan coefficient; water budget; lake evaporation; arid area

1. Introduction

Lakes are sentinels of climate change and/or human activities [1–3]. Over the past several decades, serious environmental degradation has occurred in arid northwest of China, in which the most remarkable event was a vast number of inland lakes drying up and the disappearance of aquatic

ecosystems [2,4–6]. In order to protect and restore these degraded ecosystems, the Ecological Water Conveyance Project (EWCP) in the arid inland river basin was implemented by China's government in 2000 [7,8]. For the operability of management, the EWCP identified that maintaining a certain size of lake area is an important index of whether this project has succeeded or not [9]. Yet, there has been considerable debate as to whether it is the waste or utilization for the limited water resource [9–11]. Fundamentally, the question is how much water evaporated from those lakes.

Because of the larger area of natural lakes, lake evaporation (E_L) is rarely measured directly. The most common indirect method is to multiply the measured pan evaporation (E_p) by a pan coefficient (K_p). There are many measurements of E_p from all over the world. The World Meteorological Organization [12] recommended the reference equipment as follows: the United States Class A pan, the GGI-3000 pan, and the 20 m² evaporation tank of the Russian Federation. However, this equipment cannot be found in most meteorological and hydrological stations in China; instead, the $\phi 20$ and E601 pan are used during different times and in different districts [13–15]. The E601, a modified GGI-3000 pan, appears to have consistently good performance when compared to the 20-m² evaporation tanks [14]. However, E601 has been used for less time than $\phi 20$, which was applied at most meteorological and hydrological stations over the last century in China [13]. Thus, evaporation datasets collected at different times need to be transformed into uniform times in order to determine the long-term trend of E_p [15]. Therefore, it is necessary to determine the conversion coefficients between the different types of evaporation pan.

In addition to the direct measurement by evaporation pan, models have been widely used to estimate E_p [16,17]. Although the multiple factors affect evaporation at different time scales [16,18], it has been demonstrated that the combination methods have better performance than single-variable methods when applied to estimate E_p [19–21]. However, E_L is different from E_p owing to the wall of the pan intercepts' additional radiation that enhances heat exchange, the pan edge effect that increases wind turbulence, and the oasis effect whereby the air mass of a surrounding area with lower relative humidity crosses a water body's surface and will take away more water vapor [22]. Therefore, in order to estimate the E_p precisely, Rotstayn et al. [23] developed a physical model, i.e., the PenPan model, which coupled the radiative component of Linacre [22] and the aerodynamic component of Thom et al. [24]. The PenPan model was applied successfully to estimate monthly and annual E_p of the Class A at sites across Australia [25–27] and the USA [28], and the $\phi 20$ at sites across China [29–31], but there are almost no studies reported for E601. Another alternative model to estimate E_p is reference crop evapotranspiration (ET_0) divided by a coefficient (K_c), for which a value of 0.83 was recommended [32].

We undertook a study at Juyan Lake, a typical terminal lake that is located in the lower Heihe River Basin (HRB), in the arid northwest of China [9]. It comprises the East Juyan Lake (also referred to as Sogo Nur, where the study was focused) and West Juyan Lake (also referred to as Gaxun Nur, this dried up in 1961), respectively [33]. It was famous for the discovery of a large number of Juyan bamboo slips of the Han dynasty by Sven Hedin and his partner in 1930 while they mapped the lower HRB, including Juyan Lake. To estimate E_L , the E_p of the nearest meteorological station has frequently been used [10]; however, previous studies showed drastic differences in E_p : some reported more than 3500 mm [7,34,35], but others reported less than 2500 mm [36–38]. The cause of this discrepancy was the diversity of equipment used at different times. Recently, the measured E_L by Liu et al. [10] showed that the yearly E_L was 1183.3 mm during the unfrozen period in 2014 and 2015, which suggests an overestimation of E_L using the directly measured E_p . The objectives of our study were to (1) construct a long-term and good temporal dataset of E_p by linking different types of pans through conversion coefficients; (2) identify the most appropriate model to estimate E_p ; (3) quantify the magnitude of E_L to improve the management of the lake's water resources in the hyper-arid climate, northwest China.

2. Study Area

The study area was located at the lower HRB ($39^{\circ}30'–42^{\circ}30' N$; $99^{\circ}00'–102^{\circ}00' E$, 890–1200 m a.s.l.), normally referred to as the Ejin Oasis/Delta owing to the surrounding extensive Badain Jaran and Gobi Deserts, in northwest China (Figure 1). The lower HRB starts at Zhengyixia (ZYX) hydrological station, passes through Ejin Delta, and ends at the Juyan Lake, having a length of 190 km and an area of 30,000 km² [39]. Geologically, it belongs to the Mongolian Plateau. The southwestern and northern parts of the basin are mainly formed of an alluvial plain and aggraded flood area, while the central basin consists of an alluvial plain and a lake plain. The southeastern part of the basin borders the Badain Jaran Desert [36]. The land type in the basin is similar to that of the Gobi desert except for adjacent rivers and an oasis, distributed along the Heihe River on the alluvial fan (Figure 1).

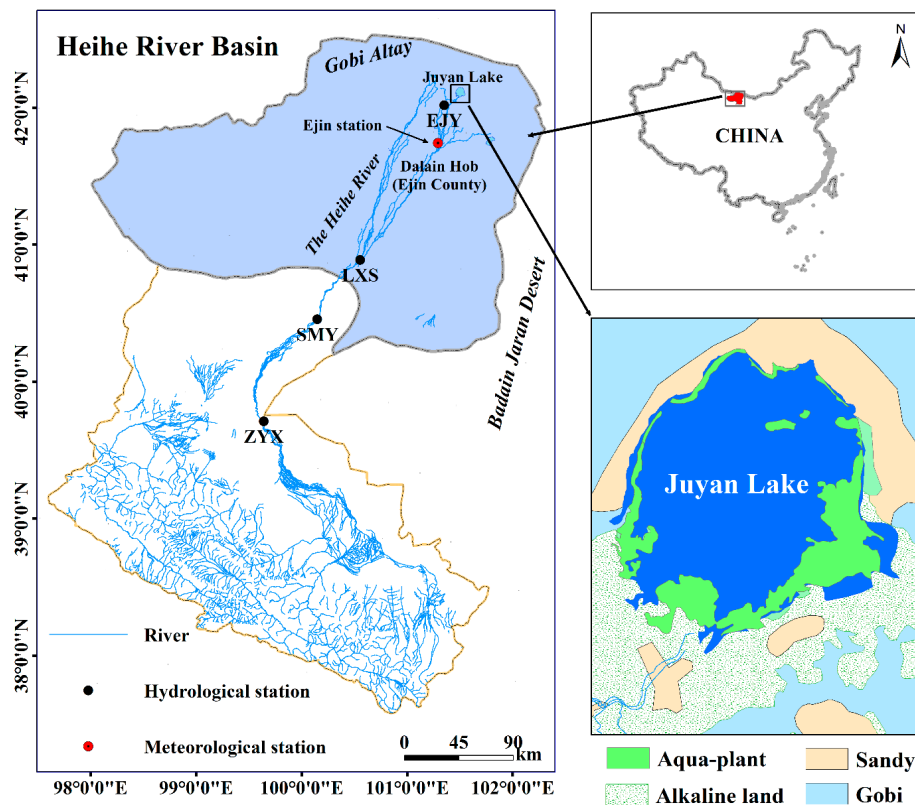


Figure 1. The schematic diagram of the Heihe River Basin, hydrological (Zhengyixia, ZYX; Shaomaying, SMY; Langxinshan, LXS; East Juyan, EJY) and meteorological station (Ejin station that located at Dalain Hob, Ejin County), the Juyan Lake and land coverage surrounding the lake.

3. Methods

3.1. Meteorological Data Collection

The Ejin County National Reference Meteorological Station ($41^{\circ}57' N$, $101^{\circ}04' E$, 940.5 m a.s.l., hereafter referred to the Ejin station) is situated in Dalain Hob, Ejin county, Inner Mongolia, about 40 km from East Juyan Lake (Figure 1). It was established in December 1956. Air temperature (T_a , °C), precipitation (P , mm), relative humidity (RH , %), wind speed (U , $m \cdot s^{-1}$), actual sunshine duration (S_d , h), and atmospheric pressure (P_a , kPa) have been collected here since 1957. Before 2002, the E_p (mm) was measured by the $\phi 20$ (20 cm diameter and 10 cm depth) in the whole year, and after 2002 by the E601 (61 cm diameter and 60 cm depth cylinder plus 8.7 cm depth circular cone) during the unfrozen period between April and October and by the $\phi 20$ during the frozen period between November and March of the next year, with a freeze–thaw transition period similar to that of the lake.

To determine the relationship between ϕ_{20} and E601, the E_p of two pans was measured synchronously during the unfrozen period from 1986 to 2001. Based on these observations, the daily and monthly ϕ_{20} and E601 datasets were used to estimate the conversion coefficient of two pans using the linear regression model following Xiong et al. [13]. After that, the E_p measured by the ϕ_{20} before 2002 was recalculated using the conversion coefficient to obtain the long-term E_p of the E601 from 1957 to 2016. The monthly variation of annual averaged P , E_p , T_a , RH and U , collected from the Ejin station, is shown in Figure S1.

3.2. PenPan Model

To estimate the E_p , the PenPan model following Rotstayn et al. [23] was used:

$$E_{PenPan} = \frac{\Delta}{\Delta + a_p \gamma} \frac{R_{n,Pan}}{\lambda} + \frac{a_p \Delta}{\Delta + a_p \gamma} f(u)(e_s - e_a), \quad (1)$$

where E_{PenPan} is the calculated E_p ($E_{p,cal}$, $\text{mm}\cdot\text{day}^{-1}$) for the Class A (unscreened), Δ is the slope of the vapor pressure curve at T_a ($\text{kPa}\cdot\text{C}^{-1}$), γ is the psychrometric constant ($\text{kPa}\cdot\text{C}^{-1}$), a_p is a constant adopted as 2.4 [22], which accounts for the additional energy exchange due to the walls of the pan, and $R_{n,Pan}$ is the daily net radiation (R_n) at the pan ($\text{MJ}\cdot\text{m}^{-2}\cdot\text{day}^{-1}$), λ is the latent heat of vaporization ($\text{MJ}\cdot\text{kg}^{-1}$), $(e_s - e_a)$ is vapor pressure deficit (kPa), $f(u)$ is the function of U at 2 m height (u_2 , $\text{m}\cdot\text{s}^{-1}$) [24]:

$$f(u) = (1.202 + 1.621u_2). \quad (2)$$

To estimate $R_{n,Pan}$, we refer to Rotstayn et al. [23]; the calculation is also provided in the Supplementary Material 6 of McMahon et al. [27]:

$$R_{n,Pan} = (1 - \alpha_A)R_{s,Pan} - R_{nl} \quad (3)$$

$$R_{s,Pan} = [f_{dir}P_{rad} + 1.42(1 - f_{dir}) + 0.42\alpha_{ss}]R_s, \quad (4)$$

where α_A is the albedo for a Class A pan given as 0.14 [23], $R_{s,Pan}$ is the total shortwave radiation received by the pan ($\text{MJ}\cdot\text{m}^{-2}\cdot\text{day}^{-1}$), R_s and R_{nl} are incoming solar radiation and net outgoing long-wave radiation, $\text{MJ}\cdot\text{m}^{-2}\cdot\text{day}^{-1}$, respectively [32]. f_{dir} is the fraction of R_s that is direct, and was defined as:

$$f_{dir} = -0.11 + 1.31 \frac{R_s}{R_a}, \quad (5)$$

where R_a is the extra-terrestrial radiation ($\text{MJ}\cdot\text{m}^{-2}\cdot\text{day}^{-1}$). P_{rad} is a pan radiation factor defined as:

$$P_{rad} = 1.32 + 4 \times 10^{-4}lat + 8 \times 10^{-5}lat^2, \quad (6)$$

where lat is the absolute value of latitude in degrees. The equations to estimate the Δ , γ , λ , $(e_s - e_a)$, R_s , R_a and R_{nl} was following FAO [32].

3.3. FAO Penman–Monteith Model

To compare with the PenPan model, the FAO Penman–Monteith model [32] was applied to calculate the ET_0 :

$$ET_0 = \frac{0.408\Delta(R_n - G) + \gamma \frac{900}{T+273} u_2 (e_s - e_a)}{\Delta + (1 + 0.34u_2)\gamma}, \quad (7)$$

where G ($\text{MJ}\cdot\text{m}^{-2}\cdot\text{day}^{-1}$) acted as the heat storage term of water bodies that can be negligible at a daily time scale. The R_n can be calculated as

$$R_n = (1 - \alpha)R_s - R_{nl}, \quad (8)$$

where α is the albedo or canopy reflection coefficient, fixed at 0.23 for the standardized reference surface (dimensionless). To compare, the relationship between R_n and $R_{n,pan}$ is shown in Figure S2. ET_0 is an alternative method that applies a K_c (a value of 0.83 was recommended) to estimate E_p following the FAO [32]:

$$ET_0 = K_c \times E_p. \quad (9)$$

3.4. Pan Coefficient and Lake Evaporation

Despite the short distance between Juyan Lake and Ejin station (Figure 1), distinct differences between their meteorological variables have been documented previously [10]. To calculate E_L , the meteorological variables T_a , RH , and U measured at the Ejin station were first recalculated according to the relationship between the two sites [10] and E_p was estimated by the selected models. Secondly, the monthly E_p was related to the measured E_L ($\text{mm} \cdot \text{month}^{-1}$) at the surface of the lake approximately 150 m from the bank during the unfrozen period of 2014 to 2015 by Liu et al. [10], and a coefficient (K_p) was calculated following Abtew [40]:

$$K_p = E_L / E_p. \quad (10)$$

Finally, the long-term E_L was calculated by applying the K_p to the estimated E_p .

3.5. Water Budget of Lake

In addition to the pan method, a water budget approach can be applied as a simple method to estimate E_L [40,41]. Because Juyan Lake is a closed lake and there is no outlet, the water budget for the lake can be written as follows:

$$\Delta S = P + Q_s + Q_g - E_L, \quad (11)$$

where ΔS is the change in lake storage (S , m^3) and Q_s and Q_g ($\text{m}^3 \cdot \text{day}^{-1}$) are the surface and ground runoff flow into the lake, respectively. The water budget was applied on an annual time scale to estimate E_L .

The Q_s inflow into Juyan Lake was measured by the weir and water level sensor that has been located at the lake inlet since August 2003 (Figure 1). To convert the unit of Q_s , $\text{m}^3 \cdot \text{day}^{-1}$ to mm and calculate the ΔS , the lake area (A_L , km^2) and S was acquired using the relationship between lake elevation and A_L and S developed by the Wuhai Hydrographic and Water Resources Survey Bureau in 2003 (Figure S3). The lake elevation has been measured at 10-day intervals since 2002 at the northeast of Juyan Lake. The maximum lake elevation was about 903.5 m and the maximum area was 42.7 km^2 in 2011. The temporal variation of 10-day measurements of S , A_L , ΔS , and Q_s was used to calculate E_L for Juyan Lake from 2002 to 2015, as shown in Figure S4.

3.6. Assessments of Model Performance

Many statistical methods, including adjusted coefficient of determination (R_{adj}^2) and root mean square error (RMSE), are used to assess E_p model performance.

$$R_{adj}^2 = \frac{\sum_{i=1}^n (X_i - \bar{X})(Y_i - \bar{Y})}{\left(\left[\sum_{i=1}^n (X_i - \bar{X}) \right]^{0.5} \left[\sum_{i=1}^n (Y_i - \bar{Y}) \right]^{0.5} \right)}, \quad (12)$$

where X_i is measured daily or monthly E_p , Y_i is estimated daily or monthly E_p , \bar{X} and \bar{Y} are mean of measured and estimated E_p , respectively. The RMSE was computed as follows:

$$\text{RMSE} = \sqrt{\frac{\sum_{i=1}^n (X_i - Y_i)^2}{n}}. \quad (13)$$

Regardless of the method used to compute the standard errors, the confidence intervals are computed using the following formula:

$$\hat{b} \pm t_{a,n-p}SE(\hat{b}), \quad (14)$$

where \hat{b} is the best-fit value for parameter b , n is the number of observations, p is the number of parameters, $SE(\hat{b})$ is the standard error of \hat{b} , and $t_{a,n-p}$ is the 100(1 - $a/2$)th percentile of the t -distribution with $n - p$ degrees of freedom. The value a is chosen so the confidence level is 100(1 - a)%. One can actually compute these statistical methods and confidence intervals in SigmaPlot (Systat Software, Inc., San Jose, CA, USA).

4. Results

4.1. Pan Evaporation of Two Types of Evaporator

During the unfrozen period from 1986 to 2001, the daily E_p measured synchronously by E601 and $\phi 20$ was ranged from 0.4 to 20.1 mm·day⁻¹ and 0.6 to 31.0 mm·day⁻¹ (Figure 2a), with an average of 9.0 mm·day⁻¹ and 13.9 mm·day⁻¹, respectively. The monthly E_p ranged from 27.9 to 361.2 mm·month⁻¹ and 41.8 to 625.9 mm·month⁻¹ (Figure 2b), with an average of 266.7 mm·month⁻¹ and 413.8 mm·month⁻¹, respectively. Whether at a daily or monthly time scale, there was a significant linear relationship between E601 and $\phi 20$ with a slope of 0.60 and 0.61 (referring to the conversion coefficients, C_p), respectively; there was less scatter at the monthly than the daily time scale within the 95% prediction band (Figure 2), which suggested that the monthly C_p may be better for reconstructing the long-term series of E_p .

Based on the estimated monthly C_p ($E_{601}/\phi 20 = 0.61$), the E_p from 1957 to 2001 measured by $\phi 20$ was converted to the E601 during the unfrozen period by multiplied by the C_p and adding the $\phi 20$ during the frozen period, and, along with the E_p measured by E601 from 2002 to 2016, the long-term E_p dataset by E601 over the past 60 years from 1957 to 2016 was established. The monthly variation of E_p and other climatic variables at Ejin station from 1957 to 2016 is summarized in Table 1. Based on the records, the annual E_p (E601) is 2240.5 mm, a figure that is greater than P (37.5 mm) by a factor of 60 (i.e., the aridity index equal to 0.02). The mean, maximum, and minimum annual T_a are 8.9 °C, 17.0 °C and -9.5 °C, respectively. The mean annual U is 3.2 m·s⁻¹ with a relatively high value in the spring. The lowest RH occurred in May with an average of 33.9%, which is the opposite of the variation of U (Figure S1). The mean annual S_d ranged from 3000 h to 3600 h, with an average of 3382 h.

Table 1. Monthly change of climatic variables included the mean (T_{mean} , °C), maximum (T_{max} , °C), minimum (T_{min} , °C) of air temperature, precipitation (P , mm), relative humidity (RH , %), sunshine duration (S_d , h), wind speed (U , m s⁻¹), and pan evaporation (E_p , mm) at Ejin station over the past 60 years (1957–2016).

Month	T_{mean}	T_{max}	T_{min}	P	RH	S_d	U	E_p
1	-11.5	-3.3	-16.9	0.3	48.7	227	2.5	35.5
2	-6.2	2.6	-12.9	0.2	36.4	231	2.8	68.4
3	2.3	10.5	-5.2	1.2	27.9	272	3.3	181.3
4	11.5	19.9	3.5	1.8	22.8	298	4.0	212.0
5	19.2	27.1	10.6	2.7	21.7	335	4.0	301.5
6	24.9	32.4	16.6	6.2	25.4	335	3.8	333.6
7	27.0	34.6	18.9	10.0	32.0	332	3.5	338.8
8	24.9	32.5	17.2	7.5	34.0	321	3.3	299.1
9	17.8	26.2	10.4	4.5	32.7	300	2.9	211.5
10	8.4	17.2	1.5	2.5	34.7	283	2.8	130.0
11	-1.7	6.4	-7.8	0.5	40.6	231	3.0	89.6
12	-9.7	-2.0	-14.9	0.3	49.5	216	2.7	39.1
Average/Sum	8.9	17.0	-9.5	37.5	33.9	3382	3.2	2240.5

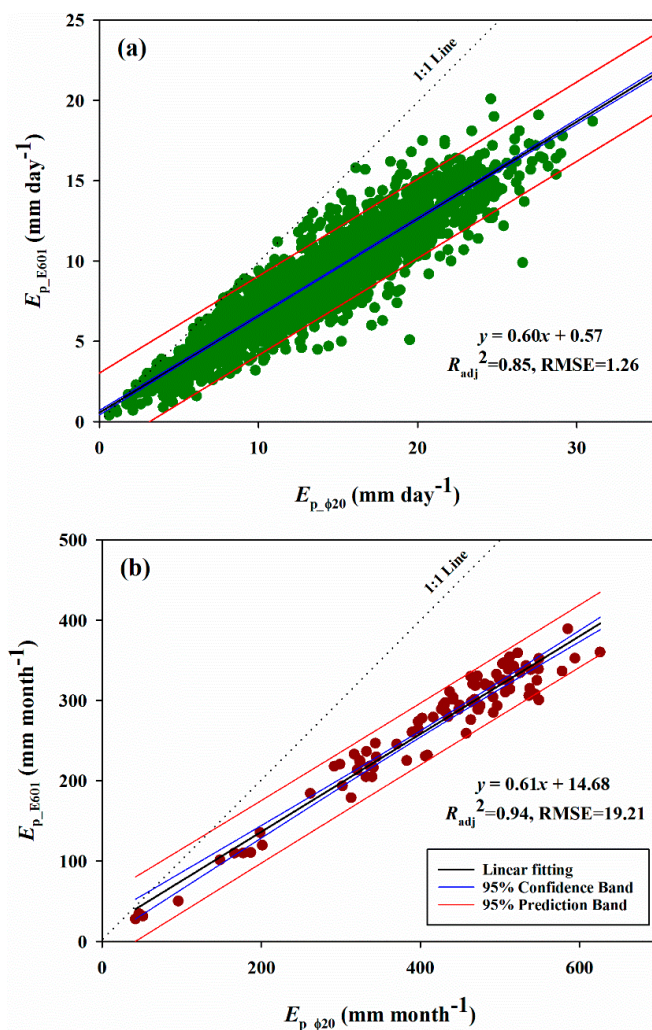


Figure 2. Relationship between pan evaporation of $\phi 20$ ($E_{p_{\phi 20}}$) and E601 ($E_{p_{E601}}$): (a) Daily ($\text{mm}\cdot\text{day}^{-1}$); (b) Monthly ($\text{mm}\cdot\text{month}^{-1}$) time scale for Ejin station during the unfrozen period from 1986 to 2001. The linear fitting, 95% confidence band, prediction band line, and value of regression analysis are shown.

4.2. Pan Evaporation Calculated by the Two Models

The relationship between the E_p observed by the evaporation pan (E601 and $\phi 20$) and calculated by the original PenPan model and modified PenPan model with the R_n recomputed following the FAO at daily and monthly time scale is shown in Figures 3 and 4, respectively. Whether at a daily or monthly scale, the E_p calculated by the original PenPan model was overestimated compared to the E601 (Figures 3a and 4a), but underestimated compared to the $\phi 20$ (Figures 3c and 4c). The calculated E_p by the modified PenPan model showed very good consistency with the E_p measured by the E601 for both of daily (Figure 3b) and monthly time scales (Figure 4b), but underestimated the E_p by the $\phi 20$ (Figures 3d and 4d). In addition, whether for the original or modified PenPan model, the calculated E_p was closer to the fitting line for the $\phi 20$ (Figures 3b,d and 4b,d) than for the E601 (Figures 3a,c and 4a,c), which was also supported by the higher R_{adj}^2 and lower RMSE for the former than the later. The scattered points were identified, focusing on the transition between the frozen and unfrozen periods, i.e., April and October (Figure 4). Similarly, E_p calculated by the FAO Penman–Monteith model was also consistent with the E_p measured by the E601 (Figure 5a), but obviously underestimated the E_p measured by the $\phi 20$ (Figure 5b). Compared to the two models, the R_n calculated by the original PenPan model was higher than by the Penman–Monteith model (Figure S2). In summary, the results

suggested that the E_p calculated by the modified PenPan model has a better performance than the original PenPan and Penman–Monteith model.

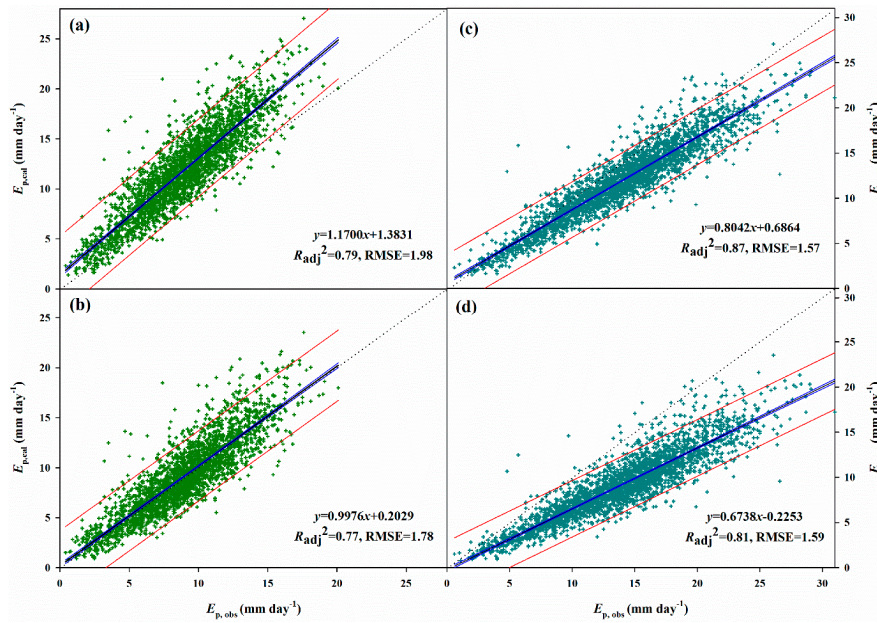


Figure 3. Relationship between daily observed pan evaporation ($E_{p,obs}$) by the E601 (a,b) and $\phi 20$ (c,d) and calculated pan evaporation by the original (a,c) and modified (b,d) PenPan model ($E_{p,cal}$) for Ejin station during the unfrozen period from 1986 to 2001. The linear fitting, 95% confidence band, prediction band line, and value of regression analysis are shown.

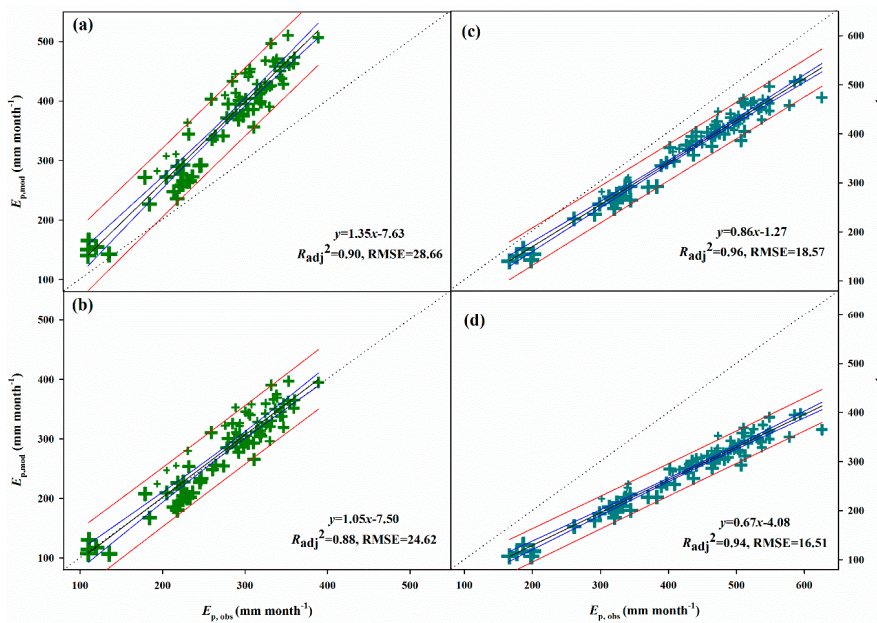


Figure 4. Relationship between monthly observed pan evaporation ($E_{p,obs}$) by the E601 (a,b) and $\phi 20$ (c,d) and calculated pan evaporation by the original (a,c) and modified (b,d) PenPan model ($E_{p,cal}$) for Ejin station during the unfrozen period from 1986 to 2001. The symbol size represents the different month: maximum for October, minimum for April, and middle for the other months. The linear fitting, 95% confidence band, prediction band line, and value of regression analysis are shown.

Based on the above, the reconstructed dataset of E_p measured by the E601 and calculated by the modified PenPan model, its radiative and aerodynamic components, and associated meteorological variables VPD and U from 1957 to 2016 are shown in Figure 6. There is an obvious declining trend of E_p , with a rate of $-6.5 \text{ mm}\cdot\text{year}^{-1}$. There are four distinct phases (highlighted by the vertical dotted lines in Figure 6): (1) increase in E_p from 1957 to 1972, at a rate of $19.0 \text{ mm}\cdot\text{year}^{-1}$; (2) decline from 1973 to 1991, at a rate of $-27.5 \text{ mm}\cdot\text{year}^{-1}$; (3) another increase from 1992 to 2009, at a rate of $24.4 \text{ mm}\cdot\text{year}^{-1}$; and (4) decrease in E_p at a rate of $-46.4 \text{ mm}\cdot\text{year}^{-1}$ during recent years. The oscillation period is roughly 18 to 20 years (Figure 6a). The yearly variations of E_p were more closely associated with the aerodynamic rather than the radiative component (Figure 6b). Specifically, the variation in E_p was consistent with U (with a linear relationship ($R_{\text{adj}}^2 = 0.63$, $p < 0.001$)) rather than with VPD (Figure 6c). On the whole, the U , VPD, calculated E_p , and its two components lagged behind the E_p of the E601.

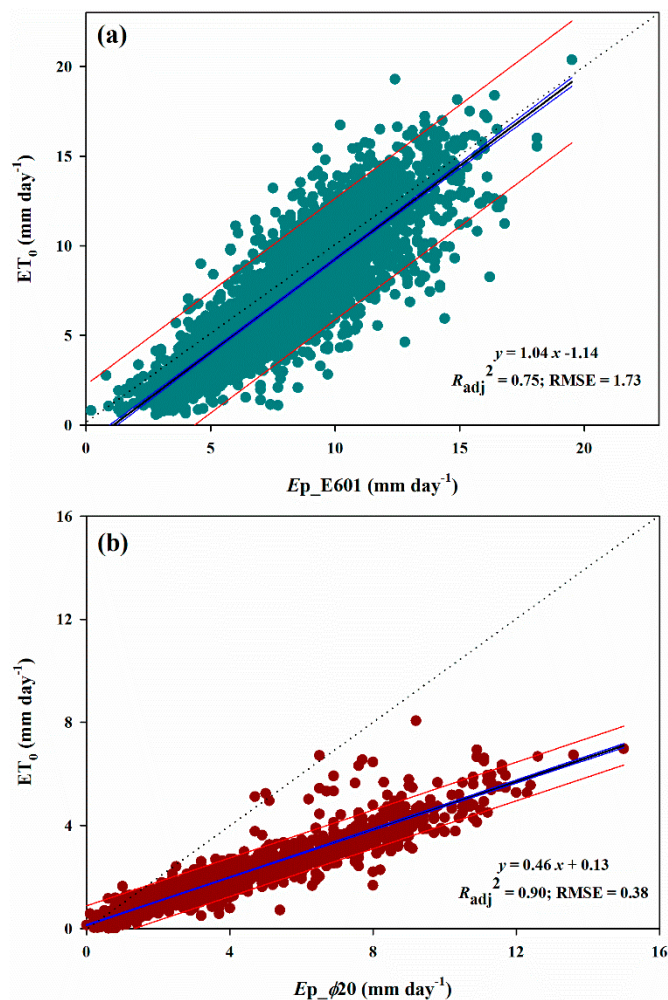


Figure 5. Relationship between daily pan evaporation of (a) E601 (E_{p_E601}) and (b) $\phi 20$ ($E_{p_φ20}$) and calculated reference crop evapotranspiration (ET_0) by the FAO Penman–Monteith equation for the Ejin station during the unfrozen period from 1986 to 2001. The linear fitting, 95% confidence band, prediction band line, and value of regression analysis are shown.

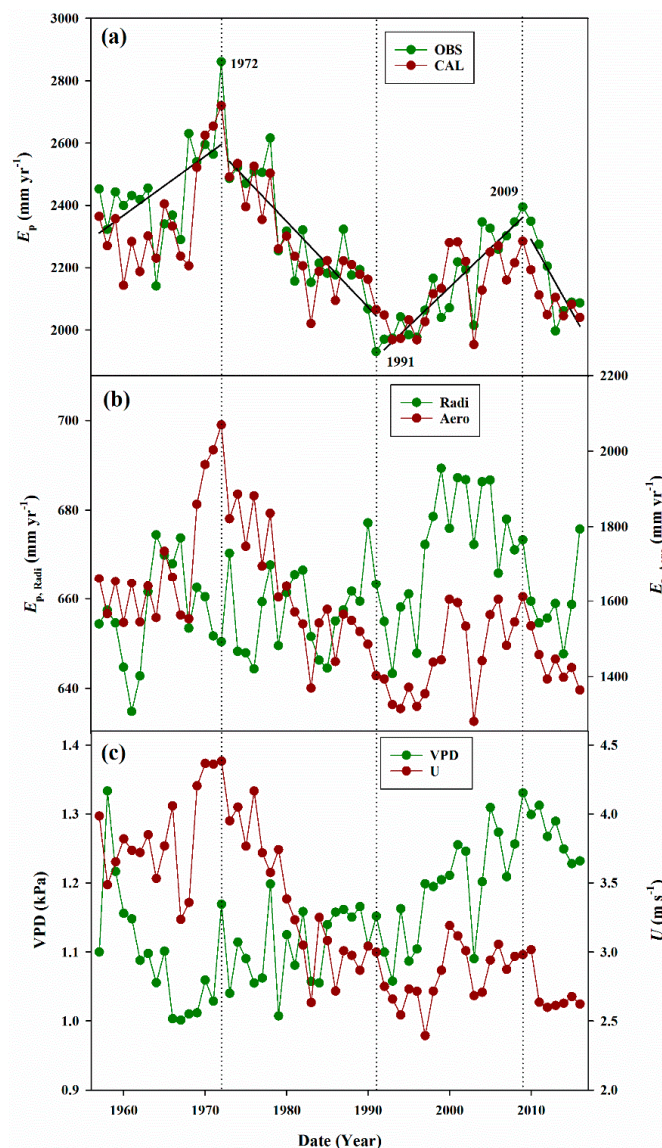


Figure 6. The reconstructed time series of (a) the observed pan evaporation (E_p , mm) by the E601 and calculated E_p by the modified PenPan model, and (b) its two components: radiative ($E_{p,Radi}$) and aerodynamic ($E_{p,Aero}$), and (c) associated meteorological variables include the vapor pressure deficit (VPD, kPa) and wind speed (U , $m \cdot s^{-1}$) for the Ejin station from 1957 to 2016. The trend line (solid) of the observed E_p by the E601 with distinctly different periods is shown in (a). The vertical (dotted) lines are the transition period of the observed E_p .

4.3. Lake Water Budget and Evaporation

The monthly water budget of Juyan Lake during the unfrozen period between 2014 and 2015 is shown in Table 2. Because the water allocation to the lower HRB was mainly focused in the summer (July) and autumn (September), Q_s and ΔS increased at the same time; inversely, ΔS decreased when there was no surface flow. The E_L of the two assessment years was approximately equivalent owing to the same lake (e.g., A_L) and meteorological (e.g., T_a , RH , and U) conditions, but the ratio of E_L to Q_s for 2015 (1.6) was twice as high as for 2014 (0.8). The K_p initially decreased and then increased with an average of 0.79 for both years, which was opposite to the variation of E_p . The calculated Q_g was associated with Q_s , i.e., discharge from the groundwater with surface flow and recharged into the groundwater without surface flow, and it was positive in 2014 but almost balanced in 2015, which suggests that Q_g can be neglected in the water budget at a yearly time scale.

Table 2. The water budget of Juyan Lake and corresponding lake and meteorological conditions during the unfrozen period in 2014 and 2015. The surface runoff (Q_s , mm), precipitation (P , mm), lake evaporation (E_L , mm), and water storage change (ΔS , mm) were directly measured and ground runoff (Q_g , mm) was calculated as a residue of the water budget. Mean of lake area (A_L , km²), air temperature (T_a , °C), relative humidity (RH , %), wind speed (U , m·s⁻¹), pan evaporation (E_p , mm), and the coefficient (K_p) of E_p to E_L are also given.

Year	Months	Q_s	P	E_L ¹	ΔS	Q_g	A_L	T_a	RH	U	E_p	K_p
2014	4	0.0	0.0	152.7	-43.2	-109.5	39.5	13.9	20.5	3.0	200.9	0.76
	5	13.1	0.0	208.7	-62.6	-133.1	39.2	19.9	18.0	3.5	277.3	0.75
	6	0.0	8.5	201.0	-75.9	-116.6	38.2	24.2	30.6	3.0	245.4	0.82
	7	519.3	2.4	216.7	124.5	180.5	39.8	28.1	29.7	2.8	293.2	0.74
	8	0.0	1.2	219.6	-136.6	-81.8	39.2	25.4	28.3	2.4	266.1	0.83
	9	866.7	0.0	180.2	345.5	341.0	38.2	18.9	30.6	2.5	207.1	0.87
Sum/Average		1399.1	12.1	1178.9	151.7	80.6	39.0	21.7	26.3	2.9	1490.0	0.79
2015	4	0.0	26.2	149.9	-156.5	32.8	40.3	13.2	26.4	2.8	175.8	0.85
	5	0.0	0.1	204.9	-127.7	-77.1	39.2	20.2	18.6	3.1	268.3	0.76
	6	0.0	3.8	209.4	-109.9	-95.7	38.2	24.4	27.6	3.3	280.4	0.75
	7	739.6	12.7	217.6	259.0	275.7	39.8	27.2	30.1	3.0	298.8	0.73
	8	0.0	0.0	224.2	-166.0	-58.2	39.2	25.9	25.2	2.9	303.9	0.74
	9	0.0	25.7	177.7	-75.9	-76.1	38.2	18.0	36.1	2.6	189.9	0.94
Sum/Average		739.6	68.5	1183.7	-376.9	1.3	39.2	21.5	27.3	2.9	1517.1	0.79

Note: ¹ Data are cited from Liu and Yu [10], and the value for April 2014 was calculated as the product of evaporation in May and the proportion of April to May in 2015.

There is a significant linear relationship (t -test, $p < 0.001$) between the measured monthly E_L and E_p during the unfrozen period, but the slope was less than 1 and the intercept was non-zero (Figure 7a), suggesting that K_p cannot be directly applied to calculate E_L by multiplying E_p . In fact, K_p varied within the year (Table 2), and was associated with U (Figure 7b). The yearly E_L from 2005 to 2015 with full lake area calculated by the water budget and the modified PenPan model ranged from 1380.5 mm to 2135.7 mm and 1206.5 mm to 1462.1 mm with an average of 1638.5 mm and 1385.6 mm, respectively (Table 3). The Q_s ranged from 309.0 mm to 2364.5 mm with an average of 1462.9 mm, which was comparable to the E_L estimated by the modified PenPan model. In addition, the E_L calculated by the modified PenPan model was consistent with the measured E_L in 2014 and 2015. The yearly E_L calculated by the water budget varied more drastically than that calculated by the modified PenPan model, especially when high surface runoff was observed (Figure 8).

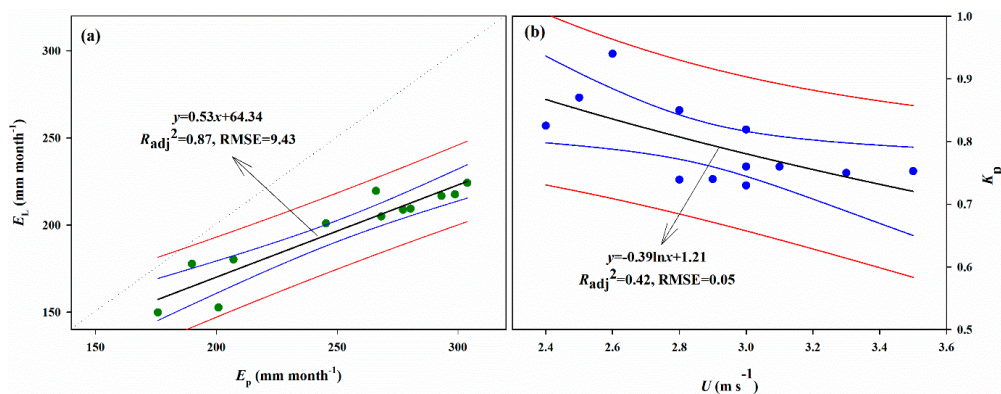


Figure 7. Relationship between (a) measured monthly lake evaporation (E_L , mm·month⁻¹) and observed pan evaporation (E_p , mm·month⁻¹) and (b) pan coefficient ($K_p = E_p/E_L$) and wind speed (U , m·s⁻¹) during the unfrozen period in 2014 and 2015. The data can be found in Table 2. The linear fitting, 95% confidence band, prediction band line, and value of regression analysis are shown.

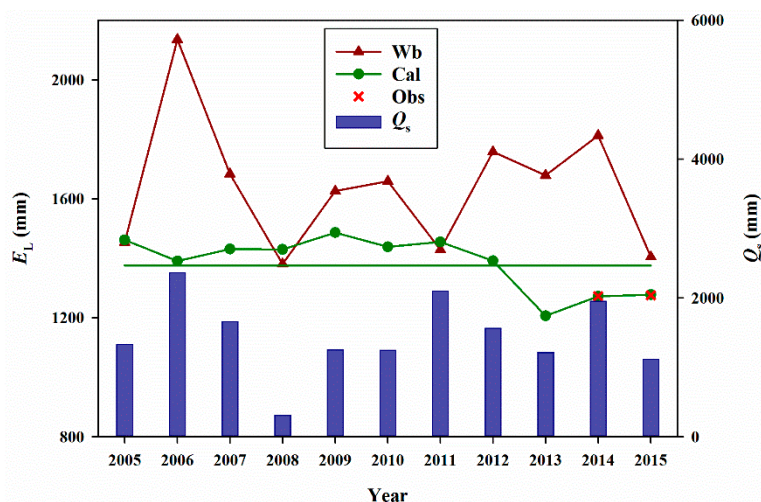


Figure 8. The yearly change of lake evaporation (E_L , mm) calculated by the water budget method (Wb) without considering the ground runoff and by the modified PenPan model (Cal) and observed E_L (Obs, 2014 and 2015) and surface runoff (Q_s , mm). The mean of E_L (straight line) calculated by the modified PenPan model is also shown.

Table 3. The yearly water budget of Lake Juyan with full water area from 2005 to 2015. The surface runoff (Q_s , mm), precipitation (P , mm), change of storage (ΔS , mm), and estimated lake evaporation by water budget (E_b , mm, equal to $Q_s + P - \Delta S$), pan evaporation (E_p , mm), coefficient (K_L) of E_b to E_p , and calculated lake evaporation (E_L , mm) by the variable K_p are shown.

Year	Q_s	P	ΔS	E_b	E_p	K_L	E_L
2005	1329.1	27.2	-97.6	1453.9	2253.5	0.65	1462.1
2006	2364.6	27.9	256.8	2135.7	2258.7	0.95	1390.7
2007	1658.9	28.0	3.0	1683.9	2301.5	0.73	1431.3
2008	309.0	63.0	-1008.5	1380.5	2346.6	0.59	1430.0
2009	1249.4	9.2	-368.0	1626.6	2394.9	0.68	1486.4
2010	1243.2	25.4	-390.7	1659.4	2348.9	0.71	1439.0
2011	2101.2	36.9	708.7	1429.4	2274.6	0.63	1455.3
2012	1558.9	32.1	-167.4	1758.4	2211.1	0.80	1391.4
2013	1213.4	34.2	-431.3	1678.9	1996.9	0.84	1206.5
2014	1949.3	16.2	152.6	1812.9	2061.8	0.88	1271.9
2015	1115.2	70.1	-218.9	1404.2	2089.5	0.67	1277.5
Mean	1462.9	31.7	-141.9	1638.5	2218.7	0.74	1385.6

5. Discussion

5.1. Pan Evaporation

For a long time, E_p has been used to gauge the evaporative demand of the atmosphere for various practical applications [27,32]. Fu et al. [14] compared E_p from numerous evaporation tanks and pans and concluded that the yearly E_p from a 100-m² evaporation tank has a distinct relationship to that of a 20-m² tank, which was about 0.99, 0.87, and 0.60 times that of the E601, Class A, and $\phi 20$, respectively. The results suggested that E_p measured by the E601 was a better approach to measuring potential evaporation than $\phi 20$. Given that, we thought the potential evaporation might be overestimated by the $\phi 20$, in which a conversion coefficient, C_p , is needed for long-term trend estimation. The monthly C_p between the E601 and $\phi 20$ (0.61, Figure 2) was comparable with that in the central region of Northern China (0.61) [15], where the study site was located for the short-term dataset. Based on the monthly C_p , the annual mean E_p (E601) was 2240.5 mm from 1957 to 2016, which was far less than the 3500 mm from 1957 to 2001 measured by the $\phi 20$ [7,34,35]. In addition, E_p estimated by the modified PenPan

model (Figures 3 and 4) and Penman–Monteith model (Figure 5) has a closer fit to the E601 than to the $\phi 20$, which suggests that the E_p measured by the E601 better represents the potential evaporation.

Because lake evaporation is different from the E_p [22], models developed for the lake evaporation are not always applicable [16,20,21]. Thus, some researchers are devoted to developing special E_p models, among which the PenPan model [22,23] was confirmed as providing better performance across Australia and the USA for Class A [25,26,28] and China for the $\phi 20$ [29–31]. Our results show that the PenPan model developed for Class A [22,23] overestimated the E601, but underestimated the $\phi 20$ (Figures 3 and 4). We thought this inconsistency was caused by the difference in estimation of R_n (Figure S2), which is the driving force of lake evaporation and a key input variable to Penman-type combination equations [42]. The consistent performance of E_p calculated by the FAO Penman–Monteith model further confirms that the R_n following the FAO was better (Figure 5). In contrast to the Class A and $\phi 20$, the E601 was embedded into the soil with its rim 30 cm above the ground and surrounded by four arc water troughs 20 cm in width that reduce the edge effects of turbulence generated by the rim of the pan [14,43]. Thus we thought the R_n above the surface of the E601 was overestimated. Irmak et al. [42] evaluated the performance of R_n estimation methods for ET_0 and reported that the FAO Penman–Monteith model (similar to Model 6) performed well against the ASCE-EWRI R_n estimating method. Therefore, we thought the better performance at estimating the E_p of the E601 by the modified PenPan model than the original PenPan and Penman–Monteith models could be attributed to the appropriate estimation of R_n above the surface of the E601.

Despite variable trends in E_p all over the world over the past 50 years [44], a decline in E_p from the 1950s to the early 1990s has been acknowledged in the arid northwest of China [13,29,45]; however, the decreased rate of E_p measured by the E601 ($-11.7 \text{ mm}\cdot\text{year}^{-1}$, 1958–1991) was higher than the mean of the northwest ($-6.0 \text{ mm}\cdot\text{year}^{-1}$) measured by the $\phi 20$ [29]. Similarly, the increased rate of E_p ($24.4 \text{ mm}\cdot\text{year}^{-1}$, 1992–2009) was higher than the mean for the northwest ($10.7 \text{ mm}\cdot\text{year}^{-1}$) [29]. While potential explanations for the decreased trends in E_p are diverse [44], our results support the conclusion that the decreased E_p was mainly induced by the weakening U [26,29,30]. This site-specific decrease in U was also confirmed at the larger spatial scale across China [46,47].

5.2. Lake Evaporation

Because of its nature, E_L is rarely measured directly, except at relatively small spatial and temporal scales [48]. Hence, the most common approach used by hydrologists or meteorologists is to apply a K_p to the measured E_p [27,40,49]. Although numerous values of K_p have been reported in the literature [32,40], most apply to Class A [20,41]. Because of the similarity of conversion coefficients of the E601 and Class A to the 20-m² evaporation tank [14], our K_p value (0.79) of the E601 (Table 2) was comparable with Class A. For example, for the second-largest completely contained freshwater lake, Lake Okeechobee in Florida, USA, Abtew [41] report monthly K_p values from 0.64 to 0.91, with an average of 0.76. For a semi-arid region like India, Ali et al. [20] reported yearly K_p values ranged from 0.65 to 0.73 with an average of 0.69. However, the fact that K_p varied seasonally (Table 2) suggests that applying a constant K_p to estimate E_L will induce large errors. It is interesting that the K_p was related to the U (Figure 7). Even though it had poor performance with a R_{adj}^2 of 0.42, it provided a way to calculate the K_p for the long term without assuming it is constant.

The yearly E_L from 2005 to 2015 with the full lake area was 1638.5 mm and 1385.6 mm, calculated by the water budget and the modified PenPan model with the variable K_p estimated by the U , respectively, i.e., the lake evaporation calculated by the modified PenPan model with the variable K_p was less than that calculated by the water budget without considering the ground runoff. The reasons for this inconsistency are: (1) the K_p can vary depending on the local environment of the pan, including pan operations or management [22], suggesting that a simple empirical relationship (Figure 7b) was insufficient to estimate E_L ; (2) the dynamic change of discharge and recharge to the groundwater may be enormous and non-ignorable, and has a large influence on the water budget of a small lake in arid and semi-arid land. Both of these reasons require further exploration.

6. Conclusions

Our study has confirmed that the PenPan model, which was developed for Class A, overestimated the E_p measured by the E601, which attribute to the overestimation of R_n . The modified PenPan model with the R_n calculated following the FAO has a better performance compared to the E_p measured by the E601. The E_L calculated by the modified PenPan model with the variable K_p was less than that calculated by the water budget method without considering the ground runoff, but consistent with the E_L measured in the short term. In summary, the linking of best pan evaporation and the best model can improve the estimation of lake evaporation and therefore water management.

Supplementary Materials: The following are available online at www.mdpi.com/2073-4441/9/12/952/s1, Figure S1: The monthly variation in mean annual meteorological variables included precipitation (P , mm), pan evaporation (E_p , mm), air temperature (T_a , °C), relative humidity (RH , %) and wind speed (U , $m \cdot s^{-1}$), Figure S2: The relationship between net radiation (R_n , $MJ \cdot m^{-2} \cdot day^{-1}$) calculated by the Penman–Monteith model (Equation (8)) and R_n of pan ($R_{n, Pan}$, $MJ \cdot m^{-2} \cdot day^{-1}$) calculated by the original PenPan model (Equations (3)–(6)) from 1957 to 2016, Figure S3: The relationship between lake elevation (m) and area (A_L , km^2) and storage (S , million m^3) of Juyan Lake, as surveyed by the Wuhai Hydrographic and Water Resources Survey Bureau, Inner Mongolia, China, in 2003, Figure S4: The time series of ten-days measured (a) lake storage (S , mm) and area (A_L , km^2), (b) change of S (mm) and surface runoff (Q_s , mm) for Juyan Lake, and (c) observed pan evaporation (E_p , mm) by the E601 (Obs) and calculated by the modified PenPan model (Cal) from 2002 to 2015.

Acknowledgments: This study was supported by the Key Research Program of Frontier Sciences, CAS (QYZDJ-SSW-DQC031), National Key R&D Program of China (2017YFC0404305), Youth Foundation of the National Natural Science Foundation of China (41401033) and the Chinese Postdoctoral Science Foundation (2014M560819). Thanks to Elizabeth A. Pinkard for her review of the paper. The authors would also like to thank the two anonymous reviewers for their constructive and valuable comments, which helped to improve this article.

Author Contributions: Teng-Fei Yu, Jian-Hua Si, Qi Feng, and Yong-Wei Chu conceived and designed the experiments; Teng-Fei Yu, Hai-Yang Xi, and Kai Li analyzed the data; Teng-Fei Yu wrote the paper.

Conflicts of Interest: The authors declare no conflict of interest. The founding sponsors had no role in the design of the study; in the collection, analyses, or interpretation of data; in the writing of the manuscript, and in the decision to publish the results.

References

- Adrian, R.; O'Reilly, C.M.; Zagarese, H.; Baines, S.B.; Hessen, D.O.; Keller, W.; Livingstone, D.M.; Sommaruga, R.; Straile, D.; Van Donk, E.; et al. Lakes as sentinels of climate change. *Limnol. Oceanogr.* **2009**, *54*, 2283–2297. [[CrossRef](#)] [[PubMed](#)]
- Ma, R.; Duan, H.; Hu, C.; Feng, X.; Li, A.; Ju, W.; Jiang, J.; Yang, G. A half-century of changes in China's lakes: Global warming or human influence? *Geophys. Res. Lett.* **2010**, *37*, L24106. [[CrossRef](#)]
- Casadei, S.; Pierleoni, A.; Bellezza, M. Integrated Water Resources Management in a Lake System: A Case Study in Central Italy. *Water* **2016**, *8*. [[CrossRef](#)]
- Yang, X.K.; Lu, X.X. Drastic change in China's lakes and reservoirs over the past decades. *Sci. Rep.* **2014**, *4*. [[CrossRef](#)] [[PubMed](#)]
- Chang, B.; He, K.N.; Li, R.J.; Sheng, Z.P.; Wang, H. Linkage of Climatic Factors and Human Activities with Water Level Fluctuations in Qinghai Lake in the Northeastern Tibetan Plateau, China. *Water* **2017**, *9*. [[CrossRef](#)]
- Wang, Y.-J.; Qin, D.-H. Influence of climate change and human activity on water resources in arid region of Northwest China: An overview. *Adv. Clim. Chang. Res.* **2017**. [[CrossRef](#)]
- Guo, Q.L.; Feng, Q.; Li, J.L. Environmental changes after ecological water conveyance in the lower reaches of Heihe River, northwest China. *Environ. Geol.* **2009**, *58*. [[CrossRef](#)]
- Cheng, G.; Li, X.; Zhao, W.; Xu, Z.; Feng, Q.; Xiao, S.; Xiao, H. Integrated study of the water–ecosystem–economy in the Heihe River Basin. *Natl. Sci. Rev.* **2014**, *1*, 413–428. [[CrossRef](#)]
- Si, J.; Feng, Q.; Yu, T.; Zhao, C. Inland river terminal lake preservation: Determining basin scale and the ecological water requirement. *Environ. Earth Sci.* **2014**, *73*, 3327–3334. [[CrossRef](#)]
- Liu, X.; Yu, J.; Wang, P.; Zhang, Y.; Du, C. Lake Evaporation in a Hyper-Arid Environment, Northwest of China—Measurement and Estimation. *Water* **2016**, *8*. [[CrossRef](#)]

11. Zhou, H.; Chen, Y.; Perry, L.; Li, W. Implications of climate change for water management of an arid inland lake in Northwest China. *Lake Reserv. Manag.* **2015**, *31*, 202–213. [[CrossRef](#)]
12. World Meteorological Organization. *Guide to Hydrological Practices Volume I Hydrology—From Measurement to Hydrological Information (WMO-No. 168)*; World Meteorological Organization: Geneva, Switzerland, 2008.
13. Xiong, A.Y.; Liao, J.; Xu, B. Reconstruction of a Daily Large-Pan Evaporation Dataset over China. *J. Appl. Meteorol. Climatol.* **2012**, *51*, 1265–1275. [[CrossRef](#)]
14. Fu, G.; Liu, C.; Chen, S.; Hong, J. Investigating the conversion coefficients for free water surface evaporation of different evaporation pans. *Hydrol. Process.* **2004**, *18*, 2247–2262. [[CrossRef](#)]
15. Li, Y.Z.; Liu, C.M.; Liang, K. Spatial Patterns and Influence Factors of Conversion Coefficients between Two Typical Pan Evaporimeters in China. *Water* **2016**, *8*. [[CrossRef](#)]
16. Singh, V.P.; Xu, C.Y. Evaluation and generalization of 13 mass-transfer equations for determining free water evaporation. *Hydrol. Process.* **1997**, *11*, 311–323. [[CrossRef](#)]
17. Altunkaynak, A. Predicting Water Level Fluctuations in Lake Michigan-Huron Using Wavelet-Expert System Methods. *Water Resour. Manag.* **2014**, *28*, 2293–2314. [[CrossRef](#)]
18. Xu, C.Y.; Singh, V.P. Dependence of evaporation on meteorological variables at different time-scales and intercomparison of estimation methods. *Hydrol. Process.* **1998**, *12*, 429–442. [[CrossRef](#)]
19. Rosenberry, D.O.; Winter, T.C.; Buso, D.C.; Likens, G.E. Comparison of 15 evaporation methods applied to a small mountain lake in the northeastern USA. *J. Hydrol.* **2007**, *340*, 149–166. [[CrossRef](#)]
20. Ali, S.; Ghosh, N.C.; Singh, R. Evaluating best evaporation estimate model for water surface evaporation in semi-arid region, India. *Hydrol. Process.* **2008**, *22*, 1093–1106. [[CrossRef](#)]
21. Winter, T.C.; Rosenberry, D.O.; Sturrock, A.M. Evaluation of 11 Equations for Determining Evaporation for a Small Lake in the North Central United States. *Water Resour. Res.* **1995**, *31*, 983–993. [[CrossRef](#)]
22. Linacre, E. Estimating U.S. Class A Pan Evaporation from Few Climate Data. *Water Int.* **1994**, *19*, 5–14. [[CrossRef](#)]
23. Rotstayn, L.D.; Roderick, M.L.; Farquhar, G.D. A simple pan-evaporation model for analysis of climate simulations: Evaluation over Australia. *Geophys. Res. Lett.* **2006**, *33*. [[CrossRef](#)]
24. Thom, A.S.; Thony, J.L.; Vauclin, M. On the proper employment of evaporation pans and atmometers in estimating potential transpiration. *Q. J. R. Meteorol. Soc.* **1981**, *107*, 711–736. [[CrossRef](#)]
25. Johnson, F.; Sharma, A. A comparison of Australian open water body evaporation trends for current and future climates estimated from Class A evaporation pans and general circulation models. *J. Hydrometeorol.* **2010**, *11*, 105–121. [[CrossRef](#)]
26. Roderick, M.L.; Rotstayn, L.D.; Farquhar, G.D.; Hobbins, M.T. On the attribution of changing pan evaporation. *Geophys. Res. Lett.* **2007**, *34*. [[CrossRef](#)]
27. McMahan, T.A.; Peel, M.C.; Lowe, L.; Srikanthan, R.; McVicar, T.R. Estimating actual, potential, reference crop and pan evaporation using standard meteorological data: A pragmatic synthesis. *Hydrol. Earth Syst. Sci.* **2013**, *17*, 1331–1363. [[CrossRef](#)]
28. Hobbins, M.; Wood, A.; Streubel, D.; Werner, K. What Drives the Variability of Evaporative Demand across the Conterminous United States? *J. Hydrometeorol.* **2012**, *13*, 1195–1214. [[CrossRef](#)]
29. Li, Z.; Chen, Y.; Shen, Y.; Liu, Y.; Zhang, S. Analysis of changing pan evaporation in the arid region of Northwest China. *Water Resour. Res.* **2013**, *49*, 2205–2212. [[CrossRef](#)]
30. Yang, H.B.; Yang, D.W. Climatic factors influencing changing pan evaporation across China from 1961 to 2001. *J. Hydrol.* **2012**, *414–415*, 184–193. [[CrossRef](#)]
31. Xie, H.; Zhu, X.; Yuan, D.-Y. Pan evaporation modelling and changing attribution analysis on the Tibetan Plateau (1970–2012). *Hydrol. Process.* **2015**, *29*, 2164–2177. [[CrossRef](#)]
32. Allen, R.G.; Pereira, L.S.; Raes, D.; Smith, M. *Crop Evapotranspiration—Guidelines for Computing Crop Requirements—FAO Irrigation and Drainage Paper 56*; FAO: Rome, Italy, 1998.
33. Nian, Y.Y.; Li, X.; Zhou, J. Landscape changes of the Ejin Delta in the Heihe River Basin in Northwest China from 1930 to 2010. *Int. J. Remote Sens.* **2016**, *38*, 537–557. [[CrossRef](#)]
34. Xi, H.; Feng, Q.; Liu, W.; Si, J.; Chang, Z.; Su, Y. The research of groundwater flow model in Ejina Basin, Northwestern China. *Environ. Earth Sci.* **2010**, *60*, 953–963. [[CrossRef](#)]
35. Si, J.H.; Feng, Q.; Zhang, X.Y.; Liu, W.; Su, Y.H.; Zhang, Y.W. Growing season evapotranspiration from *Tamarix ramosissima* stands under extreme arid conditions in northwest China. *Environ. Geol.* **2005**, *48*, 861–870. [[CrossRef](#)]

36. Li, Z.; Pan, N.; He, Y.; Zhang, Q. Evaluating the best evaporation estimate model for free water surface evaporation in hyper-arid regions: A case study in the Ejina basin, northwest China. *Environ. Earth Sci.* **2016**, *75*. [[CrossRef](#)]
37. Yu, T.F.; Feng, Q.; Si, J.H. Evapotranspiration of a *Populus euphratica* Olivier Forest and its controlling factors in the lower Heihe River Basin, Northwest China. *Sci. Cold Arid Reg.* **2017**, *9*, 175–182.
38. Wang, P.; Pozdniakov, S.P. A statistical approach to estimating evapotranspiration from diurnal groundwater level fluctuations. *Water Resour. Res.* **2014**, *50*, 2276–2292. [[CrossRef](#)]
39. Xi, H.; Zhang, L.; Feng, Q.; Si, J.; Chang, Z.; Yu, T.; Li, J. The spatial heterogeneity of riverbed saturated permeability coefficient in the lower reaches of the Heihe River Basin, Northwest China. *Hydrol. Process.* **2015**, *29*, 4891–4907. [[CrossRef](#)]
40. Abtew, W. Evaporation estimation for Lake Okeechobee in South Florida. *J. Irrig. Drain. Eng.* **2001**, *127*, 140–147. [[CrossRef](#)]
41. Jensen, M.E. Estimating evaporation from water surfaces. In Proceedings of the CSU/ARS Evapotranspiration Workshop, Fort Collins, CO, USA, 15 March 2010.
42. Irmak, S.; Odhiambo, L.O.; Mutibwa, D. Evaluating the impact of daily net radiation models on grass and alfalfa-reference evapotranspiration using the penman-monteith equation in a subhumid and semiarid climate. *J. Irrig. Drain. Eng.* **2011**, *137*, 59–72. [[CrossRef](#)]
43. Zuo, H.; Chen, B.; Wang, S.; Guo, Y.; Zuo, B.; Wu, L.; Gao, X. Observational study on complementary relationship between pan evaporation and actual evapotranspiration and its variation with pan type. *Agric. For. Meteorol.* **2016**, *222*, 1–9. [[CrossRef](#)]
44. Fu, G.B.; Charles, S.P.; Yu, J.J. A critical overview of pan evaporation trends over the last 50 years. *Clim. Chang.* **2009**, *97*, 193–214. [[CrossRef](#)]
45. Liu, X.; Luo, Y.; Zhang, D.; Zhang, M.; Liu, C. Recent changes in pan-evaporation dynamics in China. *Geophys. Res. Lett.* **2011**, *38*, L13404. [[CrossRef](#)]
46. Shi, P.J.; Zhang, G.F.; Kong, F.; Ye, Q. Wind speed change regionalization in China (1961–2012). *Adv. Clim. Chang. Res.* **2015**, *6*, 151–158. [[CrossRef](#)]
47. Guo, H.; Xu, M.; Hu, Q. Changes in near-surface wind speed in China: 1969–2005. *Int. J. Climatol.* **2011**, *31*, 349–358. [[CrossRef](#)]
48. Jones, F.E. *Evaporation of Water: With Emphasis on Applications and Measurements*; Lewis Publ., Inc.: Chelsea, MI, USA, 1992.
49. Finch, J.; Calver, A. Methods for the quantification of evaporation from lakes. In *Prepared for the World Meteorological Organization Commission of Hydrology*; CEH Wallingford: Wallingford, UK, 2008.



© 2017 by the authors. Licensee MDPI, Basel, Switzerland. This article is an open access article distributed under the terms and conditions of the Creative Commons Attribution (CC BY) license (<http://creativecommons.org/licenses/by/4.0/>).